

## Consequence modelling of large LNG pool fires on water

Steven Betteridge, Shell Research Ltd, Shell Technology Centre Thornton, P.O. Box 1, Chester, CH1 3SH

James R. Hoyes, Simon E. Gant and Matthew J. Ivings, Health and Safety Laboratory, Harpur Hill, Buxton, SK17 9JN

During the last ten years there has been a rising demand for natural gas across the World. In many countries this demand is being satisfied through an increasing number of LNG tanker deliveries and the development of new LNG import terminals. In parallel, there is a safety requirement to understand the consequences of significant accidents that would lead to the catastrophic failure of the LNG storage and hence result in a large spill of LNG in a harbour. The impact of thermal radiation on tankers, terminal facilities and the public outside the site fence-line from an LNG pool fire on water could extend a long distance according to current empirical models. In the last couple of years the World's largest LNG pool fire experiment was conducted for the US Department of Energy to quantify these hazards for pool fires up to 100 m in diameter. Some of the results of the experiment were unexpected compared to previous large scale tests (diameters 20-35 m). Specifically (1) the flames did not cover the entire area of the LNG spill, (2) the flame height was much greater than expected based on previous large scale tests and (3) soot production rates were much lower than expected.

This paper shows the latest work to understand the physical origin of these phenomena using both empirical modelling and a simple Computational Fluid Dynamics model developed using ANSYS CFX. Both approaches show that the thermal updraft generated by the fire drives a radially inward flow of air and methane from the non-burning region outside the pool fire. The velocity of this flow is predicted to be approximately  $3.5 \text{ ms}^{-1}$  and hence potentially greater than the burning velocity of the outwardly spreading pool fire. The additional air / fuel mixture being entrained into the fire may also account for the higher flame heights and reduced smoke generation.

Keywords: LNG; Pool Fire; CFD; Entrainment Velocity;

### Introduction

There is an increasing demand for natural gas, resulting in the development of new technologies such as Floating LNG (FLNG) and new LNG import terminal facilities across the world. In parallel, there is a safety requirement to understand the consequences of significant accidents that would lead to the catastrophic failure of the LNG storage. The resulting loss of containment could result in a large spill of LNG and hence a significant safety and environmental impact unless large safety distances are considered. Possible consequences include injuries or fatalities to people, property damage to the LNG ship, equipment and onshore property, and economic impacts due to long-term interruptions in the LNG supply or closure of a harbour. A number of hazard studies were used to quantify the effects for large diameter LNG pool fires in the US market, with many of these studies showing widely varying hazard consequence assessments (Blanchat *et al.*, 2011). A comparison of the safety studies showed that there was a large degree of uncertainty in the prediction of flame height, fire diameter and, importantly, the degree of smoke shielding for fires that were predicted to be up to 500 m in diameter.

The uncertainty in these results is partly due to the limited number of large scale tests that have been carried out. Until 2009, the largest pool fire test (for any fuel) was the 35 m diameter LNG pool fire test carried out at Montoir (Nedelka *et al.*, 1990). These tests clearly showed significant smoke generation and hence a reduction in the total Surface Emissive Power (SEP) of the whole flame compared to the clear burning region. In contrast, previous tests at 16 m and 20 m showed little or no smoke obscuration and demonstrated an increase in the SEP with diameter corresponding to the flame opacity reaching 100%. Altogether these results showed that the average SEP across the whole flame appears to reach a maximum value at a diameter of approximately 20 m and then decrease as the pool fire diameter is increased (Johnson, 1992). However, the actual degree of smoke obscuration as a function of pool diameter is uncertain, based as it is upon just three tests at Montoir. Empirical models that have been published subsequently use a range of correlations for SEP due to smoke obscuration, including the conservative assumption that there is no decrease in the SEP at all, e.g. the popular LNGFIRE3 model (GTI, 2004), which is used widely in the US.

The other important factor that leads to very significant differences in pool fire models is the regression rate of the liquid fuel (that is the rate of loss due to boiling/evaporation), which is normally correlated to the fire height. The regression rate has two major contributors: heat from the substrate onto which the LNG is spreading and thermal radiation from the fire above the pool. In addition, the ambient wind speed may also affect the rate of evaporation from the pool surface. This means that there is some variation in the reported values for the regression rates from LNG pool fire experiments (Raj, 2007). The highest regression rate on land was reported for the 35 m pool fire experiments at Montoir,  $0.141 \text{ kgm}^{-2}\text{s}^{-1}$  (Nedelka *et al.*, 1990). The regression rate for LNG onto water is usually considered to be higher than on land. This is because the water can effectively act as an extended heat reservoir and will therefore generate a higher boil off rate than the equivalent pool fire on land. However, the difficulty in managing LNG pool fires on water means that there is a scarcity of data; only the China Lake tests recorded the regression rate, and it was measured to be  $0.18 - 0.27 \text{ kgm}^{-2}\text{s}^{-1}$  in these tests (Raj, 1979).

To address these concerns, the US Congress funded the Department of Energy (DOE) in 2008 to conduct a series of LNG experiments at Sandia National Laboratories. The aim of the work was to address a number of current LNG spill and hazard assessment deficiencies, including assessing the potential cause and likelihood of a catastrophic release of LNG from a vessel and then any subsequent mitigation. As part of this work, two LNG spills and pool fire tests were carried out at the Sandia large scale test complex in Albuquerque in 2009 (Blanchat *et al.* 2011). The first of these produced a typical LNG pool fire with a diameter of 20 m. In the second test, however, the LNG spilled over an area with an equivalent diameter of more than 80 m but the base of the fire diameter did not extend beyond a diameter of 56 m (Figure 1). The resulting flames reached a maximum height of 146 m and produced only a superficial amount of smoke, contrary to previous results for pool fires of this size.

The present paper provides a summary of recent work to investigate the physical origin of the unexpected phenomena in the second Sandia test. Both empirical analysis and Computational Fluid Dynamics (CFD) modelling are presented to help provide an explanation for both the non-burning region and flame height.



**Figure 1:** An aerial image of Test 2 at ~ 250 s (Source: Blanchat *et al.*, 2011)

## Phoenix LNG Experiments at Sandia

The Sandia National Laboratory experimental facility was located at a latitude / longitude of North:  $34^{\circ} 58.517'$  / West:  $106^{\circ} 33.294'$ . The altitude at this location is 1630 m, which resulted in an ambient pressure of 840 – 850 mbar during both tests. The facility that was built for these tests is shown in Figure 2. The LNG was supplied to the centre of a 120 m diameter pool of water from the LNG reservoir, located in the top right of Figure 2, via three concrete pipelines with diameters 12", 24" and 36". These pipes were approximately 90 m long and were angled at 1% to allow the LNG to flow under gravity to the centre of the pool.



**Figure 2:** The experimental facility at Sandia (Source: Blanchat *et al.*, 2011)

The first experiment achieved a steady state period for approximately 200 s, with a flow rate of  $53.3 \text{ kg s}^{-1}$ . The resultant LNG pool fire had a diameter of 21.4 m and it showed typical characteristics for a fire of this size. The Shell consequence model FRED, which uses the methodology described by Johnson (1992), predicted a flame height of 33 m (taking into account the reduced pressure), and this gave good agreement to the average value that was measured during the steady state period of  $35 \pm 3$  m. The equivalent regression rate over this steady state period calculated from the flow rate and area was  $0.147 \text{ kg m}^{-2} \text{ s}^{-1}$  and was therefore slightly higher than the value recorded during the Montoir tests for a spill onto concrete.

Unfortunately, there was a high rate of boil off from the cryogenic LNG storage facilities and it was not possible to store sufficient LNG to achieve steady state conditions for the larger pool fire required in Test 2. Therefore, once Test 2 started, the LNG was released as quickly as possible. This resulted in an initial surge of LNG with a mass flow rate of up to 1600 kgs<sup>-1</sup>. A longer period of more steady flow from 140 s to 190 s followed, where the average flow rate was 800 kgs<sup>-1</sup>. However, the size of the LNG pool spill increased throughout this time period, reaching a maximum diameter of 83 m after 200 s and so a true steady state period where the pool size and flow rate were both constant was not achieved. Consequently, it was not possible to calculate an equivalent regression rate to compare to Test 1. To simplify the subsequent analysis, Table 1 gives the average flow rates in four time periods, following the opening of the plugs in the LNG reservoir at  $t = 83$  s.

The flame height increased steadily for a period of over 100 s and did not reach the maximum height of 146 m until after 220 s, by which time the LNG flow rate had reduced significantly. The extent of the burning region, which defined the pool fire diameter also increased, but not as quickly as the spreading LNG pool. The pool spill started to extend beyond the pool fire after it reached a diameter of approximately 20 m. At its maximum extent the pool fire only covered an area approximately 56 m in diameter, compared to the spill diameter of 83 m. The flame height to width ratio during this period was 2.6. During the whole experiment, only superficial smoke was seen at the top of the flame and the burning region was not obscured.

**Table 1:** Average flow rates during Test 2. The LNG was released from the reservoir at  $t = 83$  s

Time Period (s)	Flow Rate	
	m <sup>3</sup> s <sup>-1</sup>	kgs <sup>-1</sup>
83 – 123	0.16	68
123 – 141	3.79	1590
141 – 191	1.90	800
191 – 216	1.20	500

## Empirical Modelling

To understand the physical origin of this behaviour, the experimental parameters reported by Sandia (Blanchat *et al.*, 2011) were analysed using the Shell consequence tool FRED. Initial calculations of the flame height taking into account the low pressure could not predict the flame height seen during Test 2. Even assuming a pool fire diameter of 83 m (corresponding to the spill diameter), only a height of 130 m was predicted. The maximum predicted height to diameter ratio was only 1.8, which is significantly less than the 2.6 measured during Test 2.

These differences indicated that either the Thomas correlation (Thomas, 1963) for the flame height that is used in Shell FRED was no longer valid for the conditions during Test 2, or that the regression rate used in Shell FRED (0.141 kgm<sup>-2</sup>s<sup>-1</sup>) was too low. Since the Sandia Phoenix tests were on water, the regression rate is likely to be higher, and probably higher than the value calculated during Test 1. To understand the contribution to the regression rate from the water substrate, the flow rates and pool area were analysed using a transient pool model within the Shell FRED software. This model was previously validated against comparatively small releases of LNG onto concrete and it takes into account the transition from nucleation to film boiling that would be associated with releases of cryogenic liquids. In modelling Test 2, the methane was released from time  $t = 83$  s with the four release rates given in Table 1. A plot of the calculated pool area as a function of time against the measured values is given in Figure 3.

The initial prediction (solid line) gives a good prediction for both the rate of increase in pool area and for the maximum spill area, but it is offset in time from the measured values in time. This can be explained by considering that the flow rates were calculated from the change in LNG height within the cryogenic storage vessel and not the flow rates leaving the pipes 90 m away at the centre of the pool. The minimum flow velocity can be calculated by assuming simple fluid flow down the pipes, i.e. assuming no restriction at the plugs at the bottom of the reservoir and no flashing into a two-phase state (the pipe was pre-cooled with liquid nitrogen). Using an equivalent cross-sectional area of 1.59 m<sup>2</sup> (to represent the three pipes), a minimum velocity of 2.4 ms<sup>-1</sup> is required for the highest flow rate of 1590 kgs<sup>-1</sup>. The results in Figure 3 suggest that the flow speed was probably closer to 3.6 ms<sup>-1</sup>, because if the mass flow rates given in Table 1 are shifted by 25 s, then the FRED model gives excellent predictions of the spread of LNG across the water. This time correction can also be correlated with other results in the Sandia report, particularly the measurements from thermocouples placed above the centre of the pool that show a significant reduction in temperature after 150 s.

The additional time period of 25 s enables a better correlation of the LNG flow rates with the flame height measurements, so that the maximum flame height now corresponds to the end of the time period with a flow rate of 800 kgs<sup>-1</sup>. The results of the pool spill model also predict that the regression rate for LNG on water (without fire radiation) was 0.075 kgm<sup>-2</sup>s<sup>-1</sup>. This is higher than the standard boil off rate of an LNG spill on concrete 0.05 kgm<sup>-2</sup>s<sup>-1</sup> (Nova, 2005), but the difference is relatively small compared to the boil off rate for a pool fire. Consequently it confirms that the regression rate for LNG pool fires on water is dominated by radiation from the fire and not the substrate; indicating that the regression rate for Test 2 is similar to Test 1 and is approximately 0.15 kgm<sup>-2</sup>s<sup>-1</sup>.

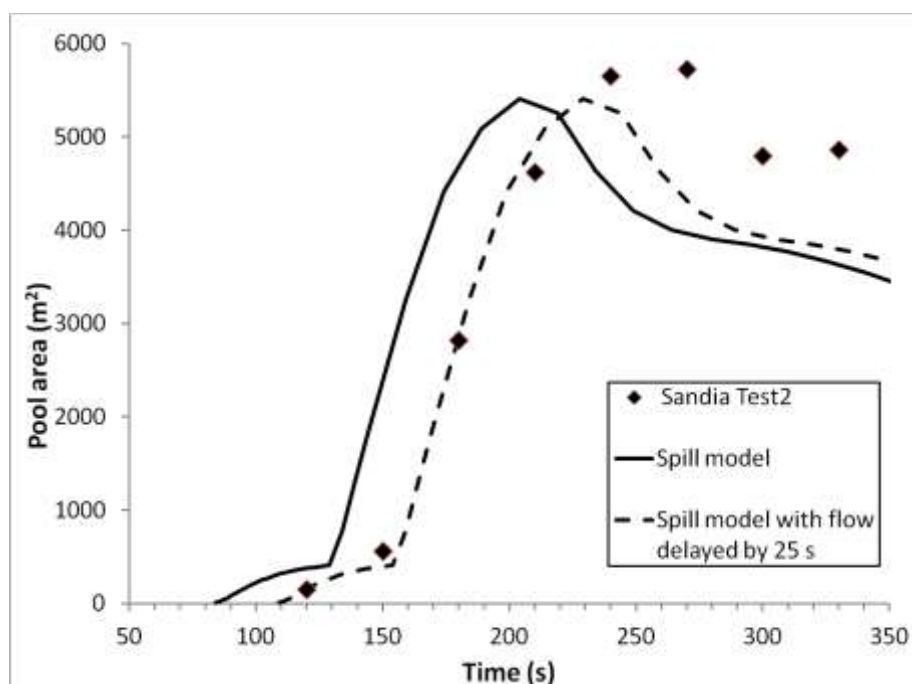


**Figure 3:** Empirical modelling of the LNG spill in Test 2 against Shell FRED

The calculated regression rates from the spill model do not help to explain the discrepancy between the measured flame height and the height predicted by the Thomas correlation. In fact, a regression rate of approximately  $0.3 \text{ kg s}^{-1} \text{ m}^2$  would be required for the Thomas correlation to predict the maximum flame height of 146 m (for a pool fire diameter of 56 m). This is more than twice that recorded in Test 1 and higher than that reported for the China lake tests (Raj 1979).

To investigate this matter further, the Thomas correlation was rearranged to output the regression rate as a function of flame height and fire diameter. Values for these quantities were taken from the Sandia report (Blanchat *et al.*, 2011) and used to produce the regression rate as a function of time, shown in Figure 4. The graph also shows (on a second vertical scale) the flow rate given in the Sandia report, which has been adjusted by 25 s to account for the delay due to the LNG flowing down the 90 m supply pipe. It is clear that there is a strong correlation between the input flow rate and the regression rate derived from the Thomas correlation, and when the input flow rate is highest, the regression rate is predicted to reach a value of  $0.5 \text{ kg m}^{-2} \text{ s}^{-1}$ . The comparison shows that a significant proportion of the input LNG is being instantaneously vaporised at this time and directly feeding the fire. After 150 s, the predicted regression rate drops to an average value of about  $0.3 \text{ kg m}^{-2} \text{ s}^{-1}$  for approximately 100 s, even though the input flow rate decreases to zero over the same time. This period between 150 s and 250 s also corresponds to a relatively stable period for recorded values of the flame height and width.

The high values of the regression rate are likely to result from additional fuel being entrained into the fire from the surrounding non-burning regions of the spill. Video recordings of Test 2 show that there is a large flow of air and vapour directed radially inwards across the non-burning region that is driven by the thermal buoyancy of the LNG fire at its centre. It could therefore be argued that the regression rate should be adjusted by the relative areas of the pool fire to the pool spill (that is, multiplied by the ratio of the pool area to the fire area because evaporation from the entire pool area appears to contribute to the fire). If a regression rate of  $0.147 \text{ kg m}^{-2} \text{ s}^{-1}$  (as determined from Test 1) is used, then this would give an adjusted regression rate of  $2.25 \times 0.147 = 0.33 \text{ kg m}^{-2} \text{ s}^{-1}$  at around 250 s, when the flame height was at its maximum. Although this is higher than predicted in Figure 4, the calculation has assumed the same regression rate across the whole pool, when in reality the regression rate could be lower near the edges of the pool spill, which are further away from the fire.

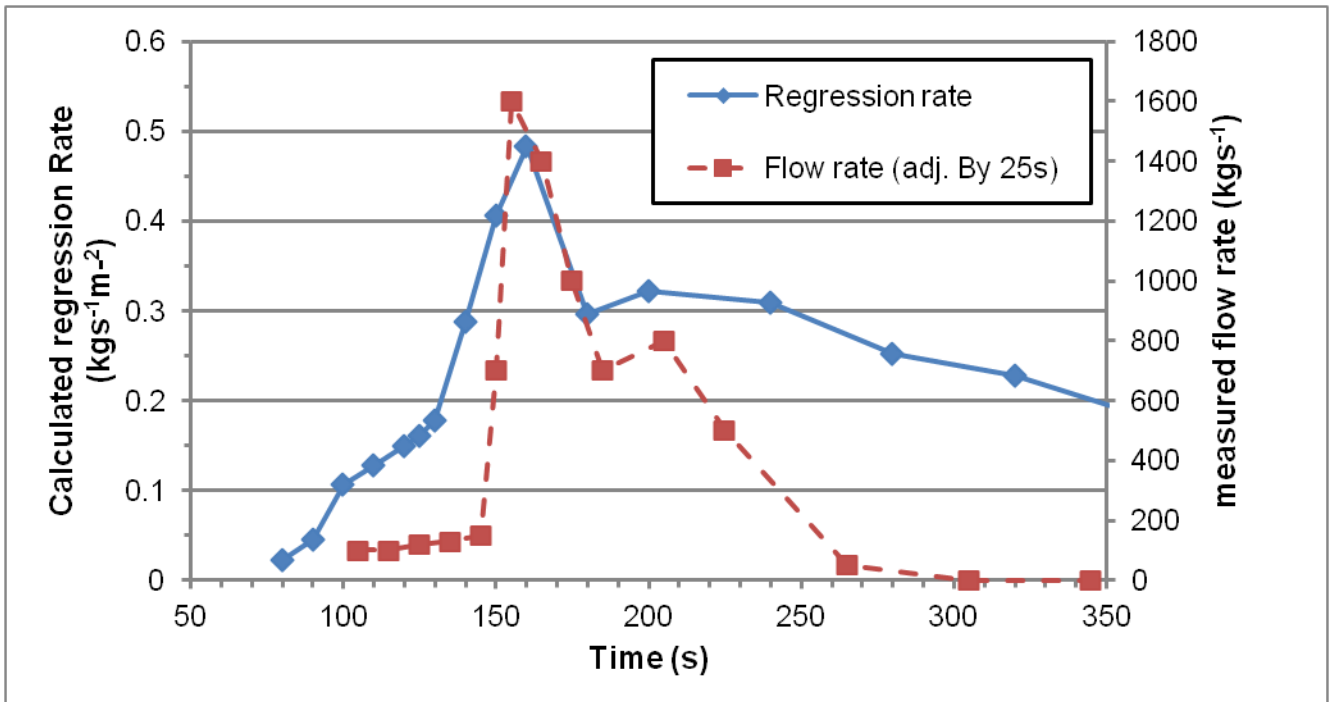


**Figure 4:** The calculated regression rate for Test 2, derived from flame height and width and using the Thomas correlation. The mass flow rate was obtained from the Sandia results (Blanchat et. al., 2011), but was adjusted by 25 s to account for travel time from the reservoir

The radially inward flow of air is also the most likely explanation for the physical process that created the non-burning area. If the entrainment velocity in the boundary layer above the surface of the LNG pool was greater than the burning velocity, then the expansion of the flame to the outer edge of the spill would be stopped. The magnitude of this entrainment velocity was analysed by tracking the positions of visible turbulent eddies in the condensation cloud within the non-burning region, using a series of individual frames from one of the videos recorded during Test 2. The positions of three of these positions are labelled A, B and C in Figure 5.

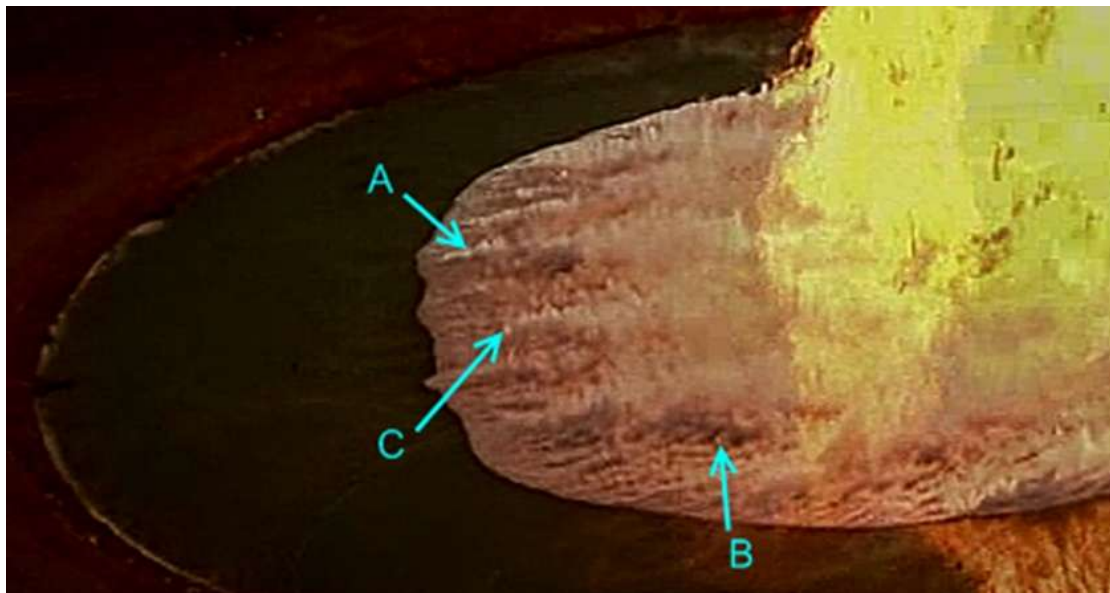


**Figure 5:** High contrast video image still of LNG Test 2 at approximately 210 s. The points marked A-C indicate the parts of the LNG plume that were tracked on a frame by frame basis. (Source Blanchat et. al., 2011)

The average radial entrainment velocity from these positions was calculated to be between 2 and 3 ms<sup>-1</sup>. This is much higher than the laminar burning velocity of around 0.4 ms<sup>-1</sup> (Lewis et al., 1961) and although turbulence will increase the burning velocity, it is interesting to note that a maximum flame spread velocity of 2 ms<sup>-1</sup> was reported for other pool fires (Gottuk et al., 2002).

To develop improved models that can predict when a non-burning region can form, either further experiments are required, or the relative magnitude of the burning velocity compared to the entrainment velocity needs to be quantified as a function of spill/fire diameter. Future large scale experiments are unlikely, especially in the medium and short term and therefore a CFD model was developed to investigate the size of both these quantities.

## CFD Modelling

CFD modelling of LNG pool fires was carried out using ANSYS CFX 14.5 (ANSYS, 2012). The aim of the CFD modelling was to investigate the non-burning regions observed during the second Sandia experiment (Blanchat *et al.*, 2011).

A computational domain was constructed that consisted of an 81 m diameter LNG pool surrounded by ground with open boundaries to the side and top. The top boundary had a height of 300 m and the side boundary was located 300 m from the centre of the fire. The fire was modelled using a volumetric heat source with a diameter of 50 m and a height of 100 m. The computational domain and volumetric heat source are shown in Figure 6.

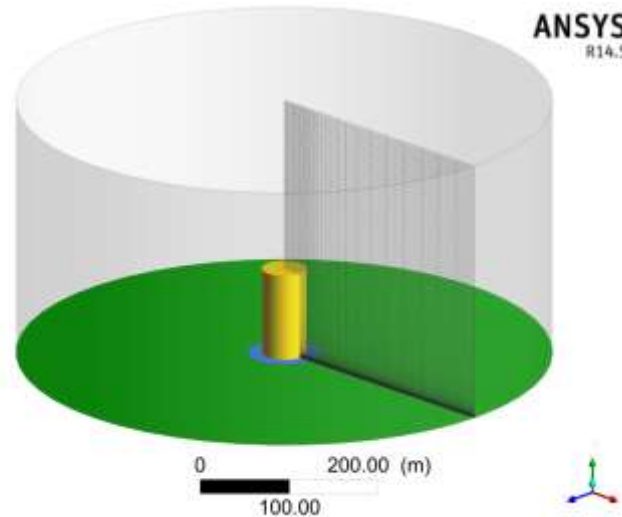


**Figure 6:** The computational domain, including LNG pool (blue), ground (green) and volumetric heat source (yellow) and mesh on a plane between the centre of the fire at  $x = 0$  and the side boundary at  $x = 300$  m.

Figure 6 also shows the structure of the computational mesh, which consisted of prism and hexahedral control volumes. Adjacent to the pool surface, the cell height was 0.01 m and in the main region of interest, in the vicinity of the volumetric heat source, the cell width in the radial direction was 1.5 m.

In the CFD model, evaporation was prescribed over the whole LNG spill area whilst “burning” was restricted to the volumetric heat source. The use of a volumetric heat source enabled non-burning regions to be simulated, which would otherwise have been difficult to simulate using a standard non-premixed combustion model (which would assume that combustion takes place everywhere the fuel vapour and air mix). The volumetric heat source released energy at a fixed rate, which was calculated from:

$$Q_c = k\Delta H\dot{m}\pi(D_p/2)^2 \quad (1)$$

where  $k$  is the combustion efficiency,  $\Delta H$  is the heat of combustion,  $\dot{m}$  is the LNG regression rate and  $D_p$  is the LNG pool diameter. Most of the simulations were carried out using a combustion efficiency of 0.7 (Heskestad, 1986) and a regression rate of  $0.147 \text{ kg m}^{-2} \text{ s}^{-1}$  (Luketa, 2011).

The LNG pool was modelled as a no-slip wall with a methane source term. Methane was released at a rate equal to the regression rate, with a temperature of  $-161^\circ\text{C}$ . The ground was modelled as an adiabatic no-slip wall, whilst the side and top boundaries were modelled as pressure openings, with a correction to account for the change in air density with height.

A number of simulations were carried out to investigate the sensitivity of predictions to the size of the computational domain, mesh resolution, height of the volumetric heat source, combustion efficiency, regression rate, turbulence intensity and surface roughness of the LNG pool. This paper describes the results from a small selection of these simulations, which are summarised in Table 2. The predictions were found to be independent of the size of the computational domain and the mesh resolution.

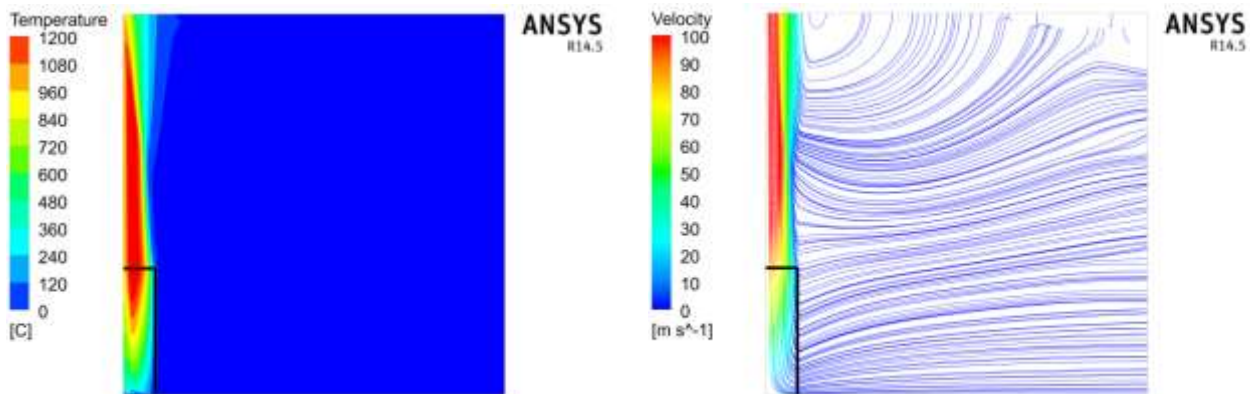
**Table 2:** Summary of CFD simulations.

Turbulence intensity at the LNG pool boundary (%)	Surface roughness on the LNG pool boundary (m)	Regression rate ( $\text{kgm}^{-2}\text{s}^{-1}$ )
10	0	0.147
100	0	0.147
1000	0	0.147
<b>1000</b>	<b>0.0002</b>	<b>0.147</b>
1000	0.005	0.147
1000	0.0002	0.126
1000	0.0002	0.21

The range of values used for the turbulence intensities of the LNG vapour source of between 10% and 1000% was selected based on the previous work of Cormier *et al.* (2009). The pool surface roughness lengths of 0.0002 and 0.005 m were chosen to represent an open sea or lake and a featureless land surface, respectively, (Weiringa, 2001). The regression rates of 0.126 and 0.21  $\text{kgm}^{-2}\text{s}^{-1}$  were recommended by Luketa *et al.* (2008) and MKOPSC (2008). The highlighted simulation in Table 1 was considered to have the most realistic input conditions for Sandia Test 2 and is therefore taken as the base case.

## CFD Results and Discussion

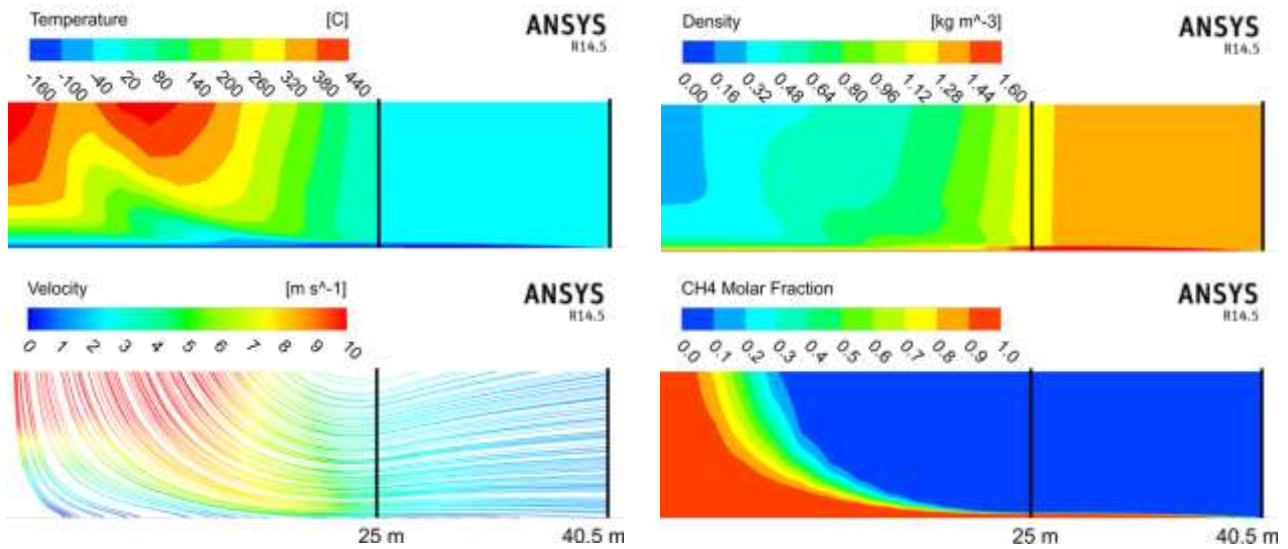
The overall behaviour of the CFD model is illustrated in the temperature and streamlines predictions shown in Figure 7. Horizontal and vertical black lines near the bottom left corner show the location of the volumetric heat source. Within this region, there is a rise in temperature, which leads to a horizontal pressure gradient that drives a flow towards the centre of the fire and up towards the top open boundary.



**Figure 7:** Temperature (left) and streamlines (right) from the base case simulation.

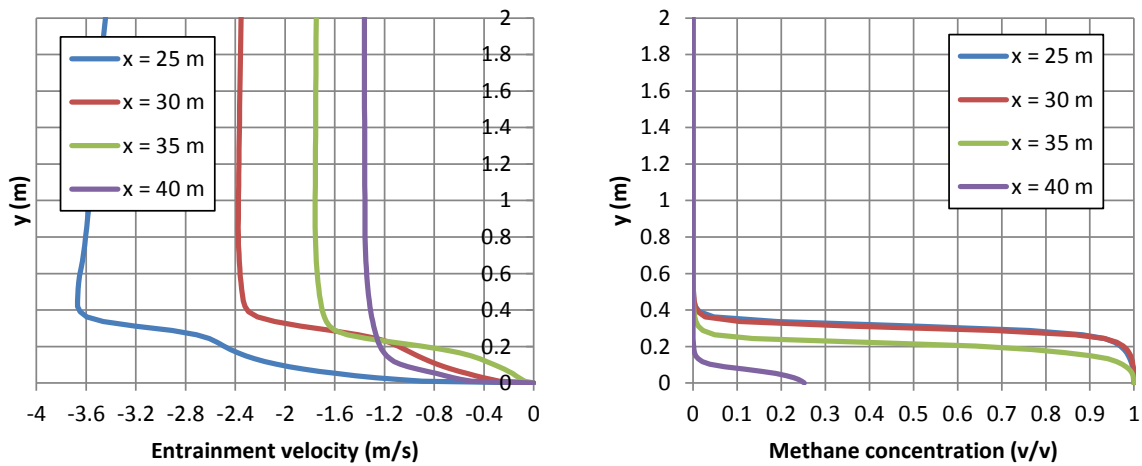
Figure 8 shows CFD model predictions of the temperature, density, streamlines and methane concentration above the surface of the LNG pool. The contour plots presented in Figure 8 cover a horizontal range of  $0 \leq x \leq 40.5$  m and a vertical range of  $0 \leq y \leq 10$  m. Vertical black lines at  $x = 25$  m and  $x = 40.5$  m denote the edge of the fire and the edge of the LNG pool spill, respectively.

The streamlines shown in Figure 8 indicate the rate at which air is entrained into the fire. Entrainment velocities vary between about  $1 \text{ ms}^{-1}$  near the edge of the pool and about  $3 \text{ ms}^{-1}$  near the edge of the fire. In addition to entraining air, the fire also entrains methane released from the non-burning regions of the LNG pool. The methane concentration contour plot shown in Figure 8 shows methane spreading along the surface of the LNG pool towards the centre of the fire.



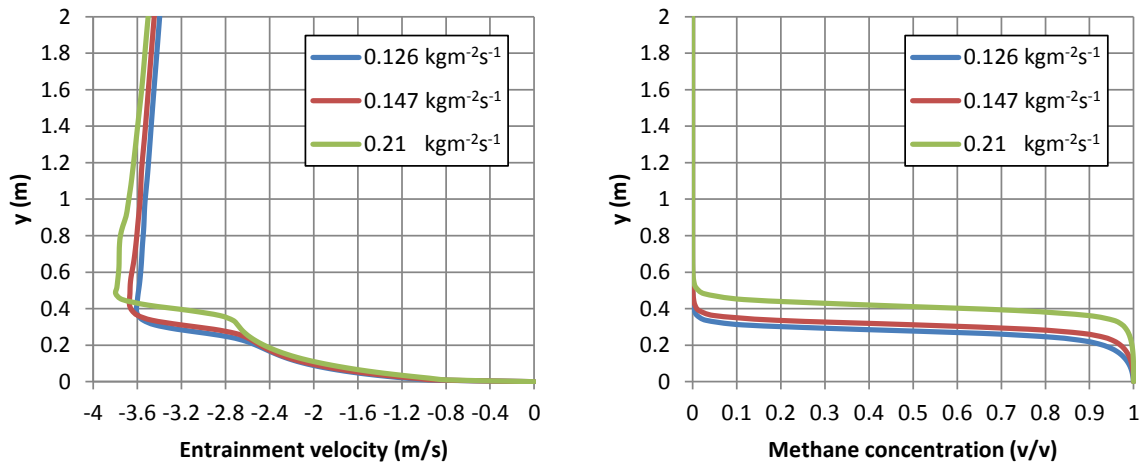
**Figure 8:** Contour plots of temperature, density, streamlines and methane concentration above the surface of the LNG pool.

Figure 9 shows the horizontal component of the entrainment velocity and methane concentration profiles at a range of radial distances between the edge of the fire and the edge of the LNG pool. The maximum entrainment velocity is predicted to increase from about  $1.4 \text{ ms}^{-1}$  near the edge of the LNG pool ( $x = 40 \text{ m}$ ) to  $3.7 \text{ ms}^{-1}$  at the edge of the fire ( $x = 25 \text{ m}$ ).



**Figure 9:** Profiles of entrainment velocity and methane concentration at  $x = 25, 30, 35$  and  $40 \text{ m}$ .

Predictions of the entrainment velocity and methane concentration in the boundary layer above the surface of the LNG pool ( $0 \leq y \leq 2 \text{ m}$ ) at the edge of the fire ( $x = 25 \text{ m}$ ) are presented in Figure 10. The results from simulations where the turbulence intensity and surface roughness were varied gave similar predictions to those from the base case.



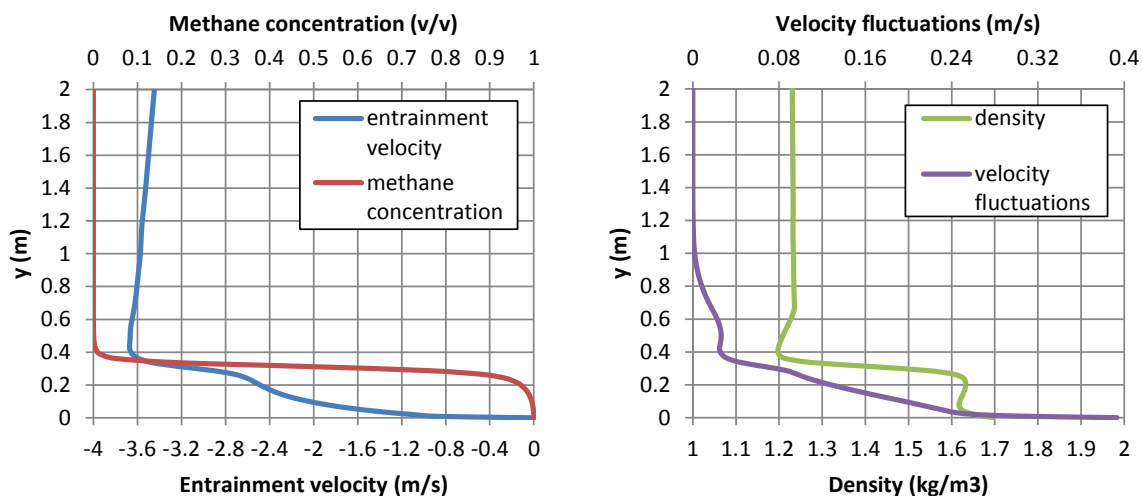
**Figure 10:** Effects of regression rate on entrainment velocity and methane concentration at  $x = 25$  m.

Figure 10 shows that the entrainment velocity and methane distribution are both sensitive to the prescribed regression rate. As the regression rate is increased, the maximum entrainment velocity increases from about  $3.6 \text{ ms}^{-1}$  to  $3.8 \text{ ms}^{-1}$ , whilst the depth of the methane rich layer increases from around  $0.3 \text{ m}$  to  $0.4 \text{ m}$ .

In each simulation there is a fairly sharp interface between the layer of methane rich gas and the air above it. Methane is flammable at concentrations of  $0.05 \text{ v/v}$  to  $0.14 \text{ v/v}$  (Lewis, 1961), which corresponds to a narrow range of heights in the CFD predictions. In the base case simulation, flammable concentrations are present over a very narrow range of heights centered on  $y = 0.35 \text{ m}$ . At this height the entrainment velocity is slightly lower than the maximum value and is approximately  $3.6 \text{ ms}^{-1}$ .

The entrainment velocity and gas concentrations are compared directly against each other in Figure 11, which also shows in a separate graph the density and velocity fluctuations in the boundary layer above the surface of the LNG pool. The cold methane gas has a higher density than the air leading to a stably stratified layer. The results show that this tends to suppress turbulence generated by the boiling LNG pool (Ohya et al., 1997).

In these simulations the fire was modelled using an idealised approach that consisted of a cylindrical volume throughout which a uniform heat source was imposed. This approach allowed a number of phenomena associated with the non-burning regions to be investigated, including methane, density, velocity and velocity fluctuation distributions in the boundary layer above the surface of the LNG pool. In a parallel programme of work, Kelsey et al. (2014) carried out simulations of LNG pool fires using the Fire Dynamics Simulator (FDS), in which they varied the fire diameter, regression rate, radiative fraction, mesh resolution and turbulence model simultaneously. FDS uses a non-premixed combustion model. It assumes that “mixed is burned” and as such, cannot predict the formation of non-burning regions. Kelsey et al. (2014) accounted for the effects of non-burning regions on the total heat release rate of the fire by increasing the regression rate up to a maximum of  $0.5 \text{ kgm}^{-2}\text{s}^{-1}$ . For a fire diameter of  $50 \text{ m}$  and a regression rate of  $0.38 \text{ kgm}^{-2}\text{s}^{-1}$  they obtained an entrainment velocity of about  $3.4 \text{ ms}^{-1}$ , which is in good agreement with the results presented here. The agreement between these two sets of results provides confidence in the predictions obtained from the two very different, but complementary modelling approaches.



**Figure 11:** Methane concentration, entrainment velocity, density and velocity fluctuations at  $x = 25$  m from the base case simulation.

## Conclusions

The second of the Sandia Phoenix LNG pool fire tests has been examined in detail, using a combination of empirical analysis and CFD modelling. This has identified that the peak in LNG supply rate to the pool occurred at the same time as the peak in the LNG regression rate, which was inferred from the measured flame height and fire diameter using the Thomas correlation. It was concluded that the very high regression rates across the fire diameter were probably due to additional fuel being entrained into the fire from the surrounding non-burning LNG spill area. If this additional fuel is taken into account, the effective regression rate of the pool fire was estimated to be approximately  $0.30 \text{ kgm}^{-2}\text{s}^{-1}$  (at the time when the maximum flame height was reached). Therefore it may be possible to characterise the height of the flame using the Thomas correlation if the regression rate is adjusted for the LNG vaporised from the non-burning region.

The video footage from Test 2 was analysed to estimate the speed at which fuel and air was entrained into the fire. At three locations roughly mid-way between the edge of the spill and the fire the entrainment velocity was estimated to be between  $2 \text{ ms}^{-1}$  and  $3 \text{ ms}^{-1}$ . These values are consistent with the results from the CFD model, presented here, which predicted entrainment velocities at the edge of the fire to be approximately  $3.6 \text{ ms}^{-1}$ , at a height of 0.35 m, where the vapour layer was within the flammable range.

These findings appear to be consistent with the hypothesis that the fire did not spread to cover the whole LNG spill surface area in Test 2 because the entrainment rate into the fire was in excess of the local burning velocity. The predicted entrainment velocities are of the order of 8 to 10 times larger than the laminar burning velocity, and larger than flame spread velocities of  $2 \text{ ms}^{-1}$  for liquid pool fires (Gottuk *et al.*, 2002). The actual burning velocity in the layer of premixed methane and air will depend on the local turbulence characteristics. Further modelling and experimental work is planned to quantify this turbulent burning velocity and thus be able to predict the extent of the non-burning area for a range of LNG spill areas.

## Acknowledgements

The photographs of Phoenix test 2 in Figures 1, 2 and 5 are taken from Blanchat *et al.* (2011), the authors would like to thank T. Blanchat, SANDIA National Laboratories for permission for their reproduction.

The HSL authors would like to acknowledge Shell Research Ltd. for funding their contribution to this research.

## References

- ANSYS (2012). ANSYS CFX-Solver Modeling Guide. ANSYS, Inc., Canonsburg, Pennsylvania, USA. Release 14.5, October 2012
- Blanchat T., Helmick P., Jensen R., Luketa A., Deola R., Suo-Anttila S., Mercier J., Miller T., Ricks A., Simpson R., Demosthenous B., Tieszen S., and Hightower M. (2011). The Phoenix series large scale LNG pool fire experiments. SAND2010-8676, Sandia National Laboratories, Albuquerque, NM.
- Cormier, B.R., Qi, R., Yun, G., Zhang, Y., and Mannan, M.S. (2009). Application of computational fluid dynamics for LNG vapor dispersion modeling: a study of key parameters. *Journal of Hazardous Materials*, 22, 332-352
- Gottuk, D.T. and White, D.A. (2002). Liquid Fuel Fires. Chapter 15, Section 2, SFPE Handbook of Fire Protection Engineering, 3rd Edition. National Fire Protection Association, Inc., Quincy, Massachusetts, USA.
- GTI (2004) Gas Technology Institute, formerly the Gas Research Institute(GRI):GTI-04/0032 LNGFIRE3: A Thermal Radiation Model for LNG Fires. Available from: <http://sales.gastechnology.org/040032.html>, accessed 10 December 2013
- Heskestad, G. (1986). Fire plume air entrainment according to two competing assumptions. 21st Symposium on Combustion, Combustion Institute, Pittsburgh, PA.
- Johnson, A.D. "A model for predicting thermal radiation hazards from large-scale LNG pool fires" 1992 *Inst. Chem Eng. Symp.Ser.*, v13, p507-57
- Kelsey, A., Gant, S.E., McNally, K. and Betteridge, S. (2014) Application of global sensitivity analysis to FDS simulations of large LNG fire plumes, IChemE Hazards 24 Conference, Edinburgh, UK, 7-9 May 2014
- Lewis, B., and von Elbe, G. (1961). Combustion, flames and explosions of gases, Second Edition. Academic Press, New York
- Luketa, A., Hightower, M. and Attaway, S. (2008). Breach and Safety Analysis of Spills Over Water from Large Liquefied Natural Gas Carriers. Sandia National Laboratories report, SAND2008-3153, May 2008
- Luketa, A. (2011). Recommendations on the Prediction of Thermal Hazard Distances from Large Liquefied Natural Gas Pool Fires on Water for Solid Flame Models. Sandia National Laboratories report, SAND2011-9415, December 2011
- Mizner G.A. and Eyre J.A., "Large scale LNG and LPG pool fires" 1982, Proceedings of the Institution of Chemical Engineering Symposium, Series No. 71, Manchester, April, 1982
- MKOPSC (2008). Mary Kay O'Connor Process Safety Center. LNG Pool Fire Modeling. White Paper. September 2008
- Nedelka D., Moorhouse, J., and Tucker, R.F., 1990 "The Montoir 35m diameter LNG pool fire experiments", Proc. 9th Int. Conf. on LNG, Nice, 17-20 Oct. 1989, Publ. by Institute of Gas Technology, Chicago

Nova Scotia Department of Energy, 2005, "Code of practice, liquefied natural gas facilities", Version 1, July 13 2005

Ohya Y, Neff D.E and Meroney R.N. 1997, "Turbulence structure in a stratified boundary layer under stable conditions", *Boundary-Layer Meteorology* 83: 139-161, 1997

Raj, P.K. et al., "Experiments Involving Pool and Vapor Fires from Spills of LNG on Water", 1979, NTIS # AD-A077073, USCG Report, Washington, DC 20590

Raj, P.K. "LNG fires: A review of experimental results, models and hazard prediction challenges" 2007, *Journal of Hazardous Materials* 140, 444-464

Thomas P.H. 1963, "The size of flames from natural fires", Ninth Symposium on Combustion Science, Academic press, New York, 844-859

Wieringa, J., Davenport, A.G., Grimmond, C.S.B. and Oke, T.R. (2001). New Revision of Davenport Roughness Classification. 3rd European & African Conference on Wind Engineering, Eindhoven, Netherlands, July 2001